

## INVESTIGATION OF RuO<sub>2</sub>-IrO<sub>2</sub>-SnO<sub>2</sub> THIN FILM EVOLUTION A thermoanalytical and spectroscopic study

Erzsébet Horváth<sup>1\*</sup>, J. Kristóf<sup>2</sup>, L. Vázquez-Gómez<sup>3</sup>, Á. Rédey<sup>1</sup> and Veronika Vágvölgyi<sup>2</sup>

<sup>1</sup>University of Veszprém, Department of Environmental Engineering and Chemical Technology, 8201 Veszprém, P.O. Box 158 Hungary

<sup>2</sup>University of Veszprém, Department of Analytical Chemistry, 8201 Veszprém, P.O. Box 158, Hungary

<sup>3</sup>Department of Chemistry, University of Ferrara, Via L. Borsari 46, 44100 Ferrara, Italy

The thermal evolution process of RuO<sub>2</sub>-IrO<sub>2</sub>-SnO<sub>2</sub> mixed oxide thin films of varying noble metal contents has been investigated under in situ conditions by thermogravimetry-mass spectrometry (TG-MS), infrared emission spectroscopy (IR) and cyclic voltammetry (CV). The gel-like films prepared from aqueous solutions of the precursor compounds RuOHCl<sub>3</sub>, H<sub>2</sub>IrCl<sub>6</sub> and Sn(OH)<sub>2</sub>(CH<sub>3</sub>COO)<sub>2-x</sub>Cl<sub>x</sub> on titanium metal support were heated in an atmosphere containing 20% O<sub>2</sub> and 80% Ar up to 600°C. Chlorine evolution takes place in a single step between 320 and 500°C accompanied with the decomposition of the acetate ligand. The decomposition of surface species formed like carbonyls, carboxylates and carbonates occurs in two stages between 200 and 500°C. The temperature of chlorine evolution and that of the final film formation increases with the increase of the iridium content in the films. The anodic peak charge shows a maximum value at 18% iridium content.

**Keywords:** electrocatalysis, IrO<sub>2</sub>, RuO<sub>2</sub>, SnO<sub>2</sub>, sol-gel process, thin films

### Introduction

Mixed oxide coatings on titanium metal support are extensively used in industrial electrochemical processes as anodes, e.g. for chlorine production [1]. Recently these types of electrochemical devices are being used to convert low-grade water into drinkable water based on faradaic effects in specially designed electrochemical cells installed at the site of consumption. For this purpose two types of treatment exist. During the 'direct' electrochemical treatment water is passed through cathodic and anodic compartments in one or more electrochemical cells. The treatment process consisting of the application of an electric field, a 'pH shock' and faradaic processes (cathodic reduction and anodic oxidation) results in the elimination of biological and chemical impurities (e.g. traces of heavy metals). The second way is an 'indirect' process in which 'neutral analytes' are produced by electrolyzing diluted brines. These analytes are then added to water allowing a complete elimination of biological and chemical impurities [2, 3]. The above technology has already found practical application but it requires improvements in cell engineering and electrode materials (especially anodic materials) [4, 5].

The improvement of these devices requires new coating materials for dimensionally stable anodes (DSAs) representing low cost and adequate service life. The most efficient method used for the preparation of mixed oxide films on metallic substrates is

the thermal decomposition of precursor salt mixtures (sol-gel method) [6]. Electrochemical and surface properties of thermally prepared oxide anodes are widely dependent on the conditions of preparation (e.g. precursor solution composition, substrate pretreatment and firing temperature) [7].

RuO<sub>2</sub>-based systems suffer from low stability, while the main disadvantage of the IrO<sub>2</sub>-SnO<sub>2</sub> binary mixtures is their high cost. The stability of RuO<sub>2</sub> can be increased with the addition of IrO<sub>2</sub> and a synergic effect of the two oxides on oxygen evolution reactions was experienced [8, 9]. However, for commercial applications the addition of a third, cheaper oxide is necessary. Recently SnO<sub>2</sub> has been used to stabilize iridium-based electrodes with good results [10]. Tin oxide also has a rutile structure and is widely used in gas sensors, solar cells and opto-electronic devices [11, 12]. There is only limited information available on the properties of RuO<sub>2</sub>-IrO<sub>2</sub>-SnO<sub>2</sub> mixed oxide coatings prepared from alcoholic solutions and on their performance in phenol oxidation [13]. Studies on the thermal evolution process have been made separately on RuO<sub>2</sub> and IrO<sub>2</sub> films stabilized by TiO<sub>2</sub>, SnO<sub>2</sub> and Ta<sub>2</sub>O<sub>5</sub> [14–18].

In the present work the thermal evolution process of the RuO<sub>2</sub>-IrO<sub>2</sub>-SnO<sub>2</sub> ternary system from aqueous precursor solutions was investigated by thermogravimetry-mass spectrometry, infrared emission spectroscopy and cyclic voltammetry.

\* Author for correspondence: elizabet@almos.vein.hu

## Experimental

### *Thin film preparation*

A Sn(IV)hydroxyacetochloride ( $(\text{Sn}(\text{OH})_2(\text{CH}_3\text{COO})_{2-x}\text{Cl}_x)$ ) solution was prepared at a concentration of 1.65 M. For this purpose  $\text{SnCl}_2 \cdot 2\text{H}_2\text{O}$  (200 g) were dissolved in deionized water (500  $\text{cm}^3$ ) subsequently adding of acetic (ethanoic) acid (200  $\text{cm}^3$ ). Small amounts of metallic tin powder and hydrogen peroxide (30%) were added slowly and the mixture was maintained for 3 days at room temperature. Then the density of the filtered solution was brought to 1.28  $\text{g cm}^{-3}$  corresponding to a tin concentration of 1.65 M [19]. In the case of the iridium precursor ( $\text{H}_2\text{IrCl}_6$ ),  $\text{H}_2\text{IrCl}_6 \cdot n\text{H}_2\text{O}$  was dissolved in deionized water with successive additions of acetic acid and 30% hydrogen peroxide, following the same procedure as for the Sn(IV) precursor, but for iridium the final concentration was 0.9 M (172.8  $\text{g Ir dm}^{-3}$ ). For the ruthenium precursor ( $\text{RuOHCl}_3$ ),  $\text{RuCl}_3 \cdot 3\text{H}_2\text{O}$  was dissolved in deionized water with successive additions of acetic acid and 30% hydrogen peroxide, following the same procedure as for the Sn(IV) precursor, but the ruthenium concentration at the end was 0.9 M (91  $\text{g Ru dm}^{-3}$ ). All precursor solutions had an acetic acid concentration of 10% (v/v). Mixtures of varying composition were made of the precursor stock solutions with noble metal contents of around 30% (molar). The following compositions were prepared:  $\text{Ru}_{0.3}\text{Sn}_{0.7}\text{O}_2$ ,  $\text{Ru}_{0.2}\text{Ir}_{0.1}\text{Sn}_{0.7}\text{O}_2$ ,  $\text{Ru}_{0.15}\text{Ir}_{0.15}\text{Sn}_{0.7}\text{O}_2$ ,  $\text{Ru}_{0.1}\text{Ir}_{0.2}\text{Sn}_{0.7}\text{O}_2$  and  $\text{Ir}_{0.3}\text{Sn}_{0.7}\text{O}_2$ . The precursor salt mixtures were deposited onto titanium metal supports (size 4 mm $\times$ 4 mm, thickness 0.3 mm). The titanium plates were sandblasted, dipped in a boiling aqueous solution of caustic soda of 1.30  $\text{g cm}^{-3}$  density for 15 min, rinsed with boiling distilled water and dried at room temperature [20]. The coatings were prepared by applying the precursor salt solution drop by drop onto the support and removing the solvent by infrared radiation (using a 250 W infrared lamp) keeping the temperature below 50°C. This procedure was repeated until a measurable quantity of the gel-like film (1–5 mg) was deposited. For the electrochemical investigations the electrode coatings were prepared with a procedure basically similar to the one described above, but the titanium strips were bigger. The calcination procedure was repeated six times with smaller amounts of solution at each deposition.

### *Thermoanalytical investigations*

Thermoanalytical investigations of the coatings were carried out in a Netzsch (Selb, Germany) TG 209 type thermobalance in a flowing gas atmosphere contain-

ing 19.8% oxygen and 80.2% argon (Messer Griesheim, Hungary). The purity of the gas mixture was 99.995%, and the heating rate was 10°C  $\text{min}^{-1}$ . In order to follow simultaneously the evolution of the gaseous decomposition products over the temperature range from ambient to 600°C, the thermobalance was connected to a Balzers MSC 200 Thermo-Cube type mass spectrometer (Balzers AG, Lichtenstein). The transfer line to introduce gaseous decomposition products into the mass spectrometer was a deactivated fused silica capillary (Infochroma AG, Zug, Switzerland; 0.23 mm o.d.) temperature controlled to 150°C to avoid condensation of high-boiling organic matter.

### *FTIR spectroscopic analyses*

Infrared emission spectroscopic measurements were performed with a Bruker Equinox 55 type FTIR spectrometer using a factory-made emission adapter. The titanium sheet with the coating on it was arranged in a vertical position and the emitted radiation from thermally excited vibrational levels was sent directly to the interferometer. The sample temperature was controlled to  $\pm 0.5^\circ\text{C}$ . The emission spectra were acquired by co-addition of 1024 scans at a resolution of 4  $\text{cm}^{-1}$  using a Peltier cooled room temperature DTGS detector.

### *Cyclic voltammetry measurements*

An Autolab PGSTAT 20 system, controlled by GPES EcoChimie software was employed for the voltammetric measurements. A platinum net was used as counter electrode and a double-walled, saturated calomel electrode (SCE), with an intermediate saturated  $\text{NaNO}_3$  solution, was used as the reference in a conventional three-electrode cell. Test solutions were prepared with deionized water using  $\text{HClO}_4$  (1 M) as support electrolyte. The electrodes were cycled for at least five times in the range between 0.15 and 1.15 V (vs. SCE).

## Results and discussion

The thermogravimetric (TG) and mass spectrometric ion intensity curves of the  $m/z=43$  ( $\text{CH}_3\text{CO}^+$ ),  $m/z=44$  ( $\text{CO}_2^+$ ) and  $m/z=70$  ( $\text{Cl}^+$ ) fragment/molecular ions of the 20% Ru–10% Ir–70% Sn ternary system are shown in Fig. 1. Interpretation of the thermal decomposition process is possible only with the continuous monitoring of the gas phase composition. By comparing the TG and MS curves it can be concluded that thermal decomposition takes place in three major steps. In the first step of decomposition water is released until 250°C (not shown for clarity). Between 110 and 190°C acetic acid fragments are detected due to the liberation of acetic acid trapped in

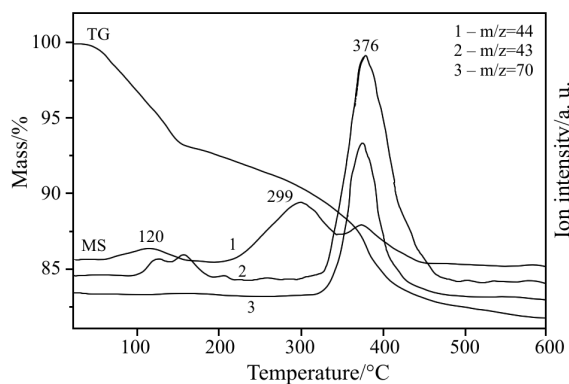


Fig. 1 TG and MS curves of the 20% Ru-10% Ir-70% Sn system

the film and to the partial decomposition of the tin precursor. The liberation of a small amount of CO<sub>2</sub> in the 60–160°C temperature range (with maximum rate at 120°C) indicates an oxidative cracking process. The absence of chlorine-containing species in the gas phase at low temperatures indicates that, unlike in alcoholic precursor solutions, intramolecular hydrolytic reactions do not occur. In the 200–320°C temperature range carbon dioxide only is formed. This is due to the decomposition (and combustion) of organic surface species connected to the noble metals. Between 320 and 480°C the final stage of decomposition (and film solidification) occurs. In this temperature range the decomposition of the acetate ligand takes place along with chlorine evolution and carbon dioxide formation. All the three processes take place simultaneously with maximum rate at 376°C.

The thermal decomposition curves of the 15% Ru-15% Ir-70% Sn system are given in Fig. 2. Changing the Ru to Ir ratio from 2:1 to 1:1 resulted in significant changes in the thermal decomposition pattern. During the first stage of decomposition, water was liberated until 190°C with maximum rate at 94°C (not shown). Trapped acetic acid is released in a broad temperature range between 48 and 193°C. High intensity carbon dioxide formation can be observed between 50 and 170°C indicating a low-temperature combustion process catalyzed by the noble metal(s). In the second stage, similarly to the previous composition, carbon dioxide is liberated only between 230 and 310°C. Since this carbon dioxide formation is due to the decomposition of organic surface species connected to the noble metal(s), the decrease of the CO<sub>2</sub> peak temperature by 34°C indicates a significant decrease in thermal stability (or a change in the nature) of the surface complexes. The chlorine evolution peak temperature in the third stage increased from 376 to 400°C. The decomposition of the acetate ligand (and the formation of CO<sub>2</sub> as a combustion product) takes place simultaneously with the formation of chlorine (between 310 and 480°C).

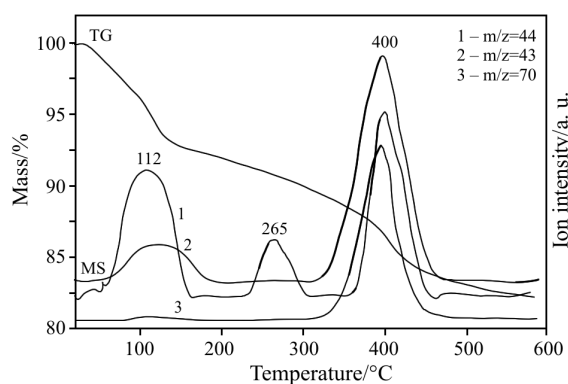


Fig. 2 TG and MS curves of the 15% Ru-15% Ir-70% Sn system

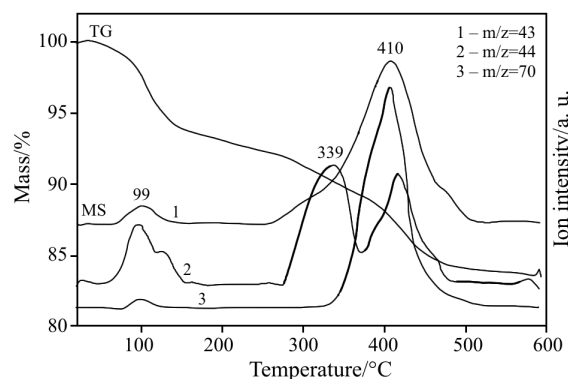


Fig. 3 TG and MS curves of the 10% Ru-20% Ir-70% Sn system

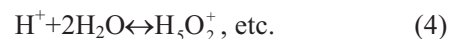
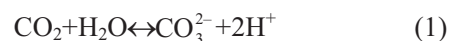
Changing the Ru to Ir ratio from 1:1 to 1:2 (10% Ru-20% Ir-70% Sn system) resulted in significant changes in the thermoanalytical curves, as well (Fig. 3). Liberation of water was observed up to 180°C with maximum rate at 98°C (not shown for clarity). Residual acetic acid was liberated at 110°C, while a small amount of chlorine formation can be observed between 70 and 130°C due to intramolecular hydrolytic reactions. It is interesting to observe that carbon dioxide is formed in two overlapping steps at approximately 99 and 140°C. Low temperature CO<sub>2</sub> formation is due to catalytic cracking reactions of complicated nature with the involvement of the noble metal(s) as catalyst(s). As to the second stage of film evolution, the decomposition of the noble metal-containing surface species takes place at higher temperatures (the peak temperature of the  $m/z=44$  (CO<sub>2</sub><sup>+</sup>) ion intensity curve increased from 265 to 339°C). At the same time, the decomposition of the acetate ligand started at 270°C (i.e. a temperature lower by 40°C than in the case of the previous composition). In the third stage, similar to the previous compositions, chlorine formation takes place simultaneously with the decomposition of the acetate ligand and the formation of carbon dioxide as decomposition/combustion product with maximum rate at 410°C. The general tendency regarding the third stage of decomposi-

tion is that while the temperature range of decomposition is broadening, the peak temperature is increasing with the increase of the iridium content.

The overall pattern of the thermal evolution process for the above compositions can be evaluated by the comparison of the TG and DTG curves in Fig. 4. Below 200°C decomposition/gas (vapour) evolution reactions take place in two overlapping stages. The second stage of decomposition takes place between 200 and 350°C. The most significant differences in the thermal behaviour of the coating compositions can be observed in the third stage between 350 and 500°C. The DTG peak maxima show a gradual shift to higher temperatures with the increase of the iridium content. A similar tendency can be observed in the final film solidification temperature, as well.

The emission infrared (IRES) spectra of the precursors as well as of the 20% Ru+10% Ir+70% Sn and the 10% Ru+20% Ir+70% Sn ternary systems at 200°C are shown in Fig. 5. Assignment of the bands is given in Table 1. In the 2200–1300 cm<sup>-1</sup> spectral range the presence of carbonyl-, carboxyl- and car-

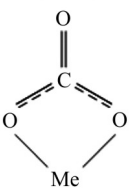
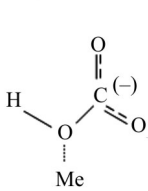
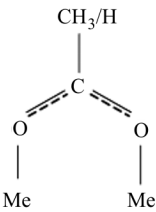
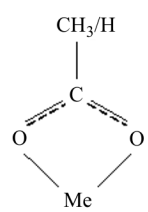
bonate-type surface species can be identified. CO and CO<sub>2</sub> are the oxidation products of the acetate ligand and can react with water as follows:



The spectra of the two ternary systems show close similarity. At lower iridium content, however, the relative intensities of the carbonyl and carboxylate bands and those of the Zundel-type complexes (e.g. H<sub>5</sub>O<sub>2</sub><sup>+</sup>) are higher. The C–H stretching vibration bands of the organic species above 200°C are rather weak, while those of the bending vibrations overlap with the carbonate and carboxylate bands.

The amount of the anodic peak charge determined by cyclic voltammetry (CV) is proportional to the number of surface active sites available in the electrochemical reaction. Figure 6 shows the change of the

**Table 1** Assignment of IR bands (cm<sup>-1</sup>) and the schematics of the proposed surface structures

Spectral band/cm <sup>-1</sup>	Type of surface species	Structure [22–26]
2120 1916 1832	linear	$\text{V}_{\text{C}=\text{O}}$ Me–O...C≡O coordinatively bonded CO
1708		$\text{V}_{\text{C}=\text{O}}$ $\text{V}_{\text{C}=\text{O}}$ acetic acid bridging bidentate
1612 1521	bidentates bicarbonates	$\text{V}_{\text{as}(\text{O}-\text{C}-\text{O})}$ <div style="display: flex; justify-content: space-around; align-items: center;"> <div style="text-align: center;"> <p>bidentate</p>  </div> <div style="text-align: center;"> <p>bicarbonate</p>  </div> </div>
1488 1430	carboxylates	bridged bidentate carboxylates <div style="display: flex; justify-content: space-around; align-items: center;"> <div style="text-align: center;"> <p>CH<sub>3</sub>/H</p>  </div> <div style="text-align: center;"> <p>CH<sub>3</sub>/H</p>  </div> </div>
1430–1404 1354 1302		$\beta_{\text{C}-\text{H}}$ $\delta_{\text{s}(\text{CH}_3)}$ $\text{V}_{\text{s}(\text{O}-\text{C}-\text{O})}$ organic species acetic acid fragments
1257	bidentates	$\text{V}_{\text{s}(\text{C}=\text{O})}$ C–H bending bridging bidentate organic species
1105–909 800–600	Zunder structure	H <sub>5</sub> O <sub>2</sub> <sup>+</sup> Me-oxides

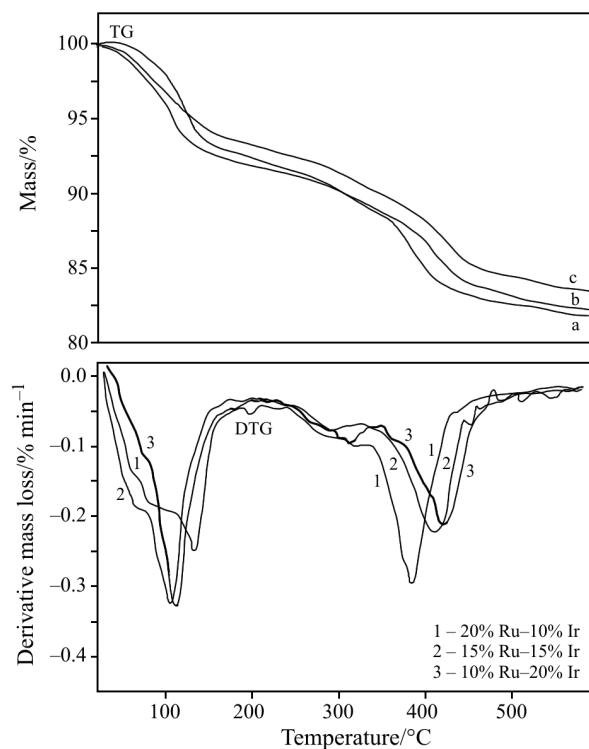


**Fig. 4** TG and DTG curves for the prepared mixtures;  
 a – 20% Ru–10% Ir–70% Sn  
 b – 15% Ru–15% Ir–70% Sn and  
 c – 10% Ru–20% Ir–70% Sn

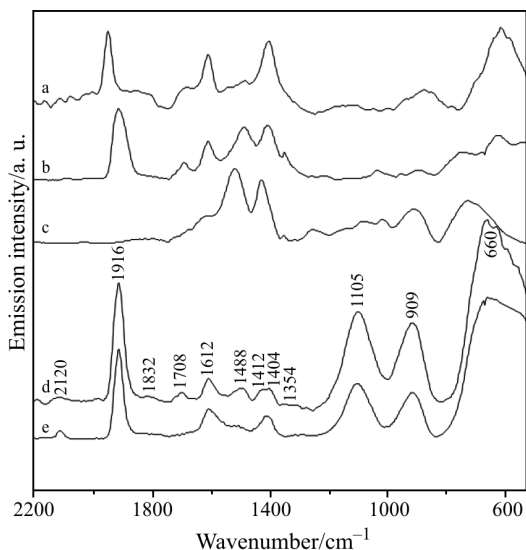


**Fig. 5** IR spectra of the coatings heated at 200°C;  
 a – 100% Ir, b – 100% Ru, c – 100% Sn,  
 d – 20% Ru+10% Ir+70% Sn and  
 e – 10% Ru+20% Ir+70% Sn

anodic charge – as coulomb per mmol noble metal ( $C\text{ mmol M}^{-1}$ ) – as a function of the film composition. The total charge capacity was estimated from CV curves recorded at a potential sweep rate of  $10\text{ mV s}^{-1}$ . The contribution due to the outermost part of the films

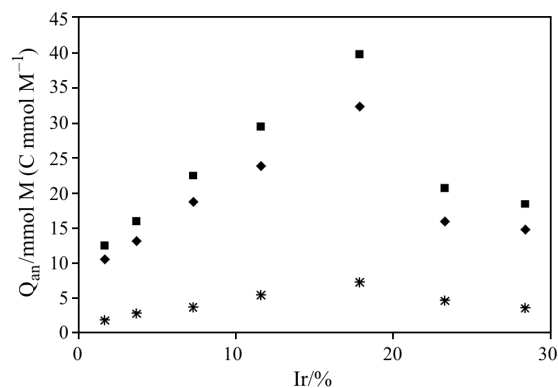


**Fig. 6** Dependence of the voltammetric charges on electrodes composition in 1 N HClO<sub>4</sub>; ■ – total anodic charge, ♦ – external anodic charge, \* – internal anodic charge

was estimated directly from CV curves obtained at  $600\text{ mV s}^{-1}$ . The internal anodic charge was determined by the difference of the two sets of figures [21]. Figure 6 shows that the anodic charge is maximum at 18% iridium content. At this composition the rate of gas evolution through the solidifying surface layer is high, resulting in cracks and pores in the outermost part of the film leading to a higher surface area. The broader range of thermal decomposition as well as an increase of the gas evolution peak temperature can also contribute to the increase of the number of the active sites at the surface. The fact that the internal anodic charge can also contribute (to a little extent) to the total anodic charge indicates that not only the outermost, but also some of the inner layers can take part in the electrode processes.

## Conclusions

The complicated decomposition reactions of the precursor coatings prepared onto titanium support can only be followed with the continuous monitoring of the gas phase composition by thermogravimetry combined with mass spectrometry. In addition, the vibrational spectroscopic identification of surface species formed on heating is indispensable to completely characterize the subtle process of thin film evolution. The information obtained on the nature of decomposition reactions, the temperature ranges of formation/decomposition of the surface species as well as on the final temperature of mixed oxide film formation can be advantageously used in the design and preparation of real electrodes. Since the electrocatalytic activity of the final oxide films depends strongly on the surface properties, the in situ study of film evolution can be advantageously used to find correlations between surface characteristics and preparation conditions.

## Acknowledgements

This research was supported by the Hungarian Scientific Research Fund (OTKA) under grant No. K62175.

## References

- 1 S. Trasatti (Ed.), *Electrodes of Conductive Metals Oxides*, Elsevier, Amsterdam, Part A, 1980; Part B, 1981.
- 2 A. P. Tomilov, *Zhizn Bezopasnost*, 3 (2002) 302.
- 3 R. N. Borwick, R. J. Stoland, S. C. Robinson, V. M. Bakhir and J. G. Zadorozhny, *International Patent Registration Number WO98/013304 A1*, 29 September 1997.
- 4 V. M. Bakhir, J. G. Zadorozhny and T. Barabash, *U. S. Patent No. 5871623*, 16 February 1999.
- 5 K. Jüttner, U. Galla and H. Schmieder, *Electrochim. Acta*, 45 (2000) 2575.
- 6 R. Reisfeld and C. K. Jørgensen (Eds), *Chemistry, Spectroscopy and Applications of Sol-Gel Glasses*, Springer-Verlag, Berlin 1992.
- 7 R. R. L. Pelegrino, L. C. Vicentin, A. R. De Andrade and R. Betazzoli, *Electrochem. Commun.*, 4 (2002) 139.
- 8 F. I. Mattos-Costa, P. de Lima-Neto, S. A. S. Machado and L. A. Avaca, *Electrochim. Acta*, 44 (1998) 1515.
- 9 Y. E. Roginskaya, T. V. Varlamova, M. D. Goldstein, I. D. Belova, B. Sh. Galyamov, R. R. Shifrina, V. A. Shepelin and V. N. Fateev, *Mater. Chem. Phys.*, 30 (1991) 101.
- 10 B. Correa-Lozano, Ch. Comminellis and A. De Battisti, *J. Appl. Electrochem.*, 27 (1997) 970.
- 11 W. Gobel and K. D. Schierbaum, *Sens. Actuators B*, 2627 (1995) 1.
- 12 P. P. Tsai, I. C. Chen and M. H. Tzeng, *Sens. Actuators B*, 2425 (1995) 537.
- 13 M. E. Makgae, C. C. Theron, W. J. Przybylowicz and A. M. Crouch, *Mater. Chem. Phys.*, 92 (2005) 559.
- 14 A. De Battisti, G. Battaglin, A. Benedetti, J. Kristóf and J. Liszi, *Chimia*, 49 (1995) 17.
- 15 J. Kristóf, T. Szilágyi, E. Horváth and R. L. Frost, *Thin Solid Films*, 485 (2005) 90.
- 16 J. Kristóf, S. Daolio, A. De Battisti, C. Piccirillo, J. Mihály and E. Horváth, *Langmuir*, 15 (1999) 1498.
- 17 E. Horváth, J. Kristóf, R. L. Frost, N. Heider and V. Vágvölgyi, *J. Therm. Anal. Cal.*, 78 (2004) 687.
- 18 J. Kristóf, T. Szilágyi, E. Horváth, A. De Battisti, R. L. Frost and Á. Rédey, *Thermochim. Acta*, 413 (2004) 93.
- 19 A. Morozov, A. De Battisti, S. Ferro and G. N. Martelli, *International Patent Registration Number WO2005/014885 A1*, 17 February 2005.
- 20 A. Morozov, A. De Battisti, S. Ferro and G. N. Martelli, *International Patent Registration Number WO2005/014884 A2*, 17 February 2005.
- 21 S. Ardizzone, G. Fregonara and S. Trasatti, *Electrochim. Acta*, 35 (1990) 263.
- 22 E. Horváth, J. Kristóf, E. Jakab, É. Makó and V. Vágvölgyi, *J. Colloid Interface Sci.*, 289 (2005) 132.
- 23 K. Tanaka, K. L. Watters and R. F. Howe, *J. Catal.*, 75 (1982) 23.
- 24 G. B. McVicker, R. L. Baker, R. L. Garter and E. L. Kugler, *J. Catal.*, 65 (1980) 207.
- 25 A. Erdőhelyi, K. Fodor and G. Suru, *Appl. Catal. A General*, 139 (1996) 131.
- 26 P. S. Braterman, *Metal Carbonyl Spectra*, Academic Press, London 1975, p. 202.

---

OnlineFirst: August 11, 2006

---

DOI: 10.1007/s10973-006-7578-2